Original Research

Tumor Microvascular Changes in Antiangiogenic Treatment: Assessment by Magnetic Resonance Contrast Media of Different Molecular Weights

Karl Turetschek, MD,[1,2] Anda Preda, MD,[1,3] Viktor Novikov, MD,[1] Robert C. Brasch, MD,[1] Hanns J. Weinmann, PhD,[4] Patrick Wunderbaldinger, MD,[2] and Timothy P.L. Roberts, PhD[1,5]*

Purpose: To test magnetic resonance (MR) contrast media of different molecular weights (MWs) for their potential to characterize noninvasively microvascular changes in an experimental tumor treatment model.

Materials and Methods: MD-MBA-435, a poorly differentiated human breast cancer cell line, was implanted into 31 female homozygous athymic rats. Animals were assigned randomly to a control (saline) or drug treatment (monoclonal antibody vascular endothelial growth factor (Mab-VEGF) antibody) group. In both groups, dynamic MR imaging (MRI) was performed in each animal using up to three different contrast media on sequential days at baseline and follow-up examination. The MWs of the contrast media used ranged from 557 Da to 92 kDa. Using a bidirectional kinetic model, tumor microvessel characteristics, including the fractional plasma volume (fPV) and transendothelial permeability (K^{PS}), were estimated for each contrast medium. These microvascular characteristics were compared between drug and control groups and between contrast media of different MWs.

Results: Tumors grew significantly slower ($P < 0.0005$) in the drug treatment group than in the control group. Mean K^{PS} and fPV values decreased significantly ($P < 0.05$) in the Mab-VEGF antibody-treated group compared to baseline values using intermediate or macromolecular contrast media (MMCM), but did not change significantly using small molecular contrast media (SMCM). In the control groups, mean K^{PS} and mean fPV values did not reach statistical significance for any of the contrast media used.

Conclusion: Therapeutic effects of a Mab-VEGF antibody on tumor microvessel characteristics can be monitored by dynamic MRI. Intermediate-size agents, such as Gadomer-17, offer a substantial dynamic range and are less limited by imaging precision and therefore should be considered a practical alternative to monitor antiangiogenesis treatment effects in a clinical setting.

Key Words: magnetic resonance imaging; angiogenesis; vascular endothelial growth factor; contrast media; permeability
J. Magn. Reson. Imaging 2004;20:138–144.

TUMOR NEOVASCULARIZATION is crucial for cancer growth and therefore directly influences patient prognosis. The close relationship between tumor angiogenesis, the metastatic potential of malignant tumors, and, finally, patient survival has already been shown in numerous studies (1–5). Recent advances in the development of angiogenesis inhibitors have led to new forms of tumor treatment. Many drugs are currently under preclinical investigation to test their individual potential to stop, reverse, or at least slow down tumor growth (6–10). Although different drugs target tumor angiogenesis at different molecular levels, all of them have in common various morphological changes of the tumor microvasculature: these include apoptosis (11,12), changing the microvascular permeability by loosening endothelial tight junctions (13), increasing the number of transcellular channels or vesiculovacuolar organelles (VVOs) (14), and more.

Dynamic magnetic resonance imaging (MRI), used in combination with macromolecular contrast media (MMCM) and kinetic modeling, has shown the potential to monitor changes in the tumor microvasculature following antiangiogenic therapy by determination of microvessel parameters, such as transendothelial permeability (K^{PS}) or fractional plasma volume (fPV) (15–17). In these studies small molecular contrast media (SMCM), i.e., gadopentetate (GdDTPA), failed to differentiate reliably between pre- and post-drug-induced changes of microvessel characteristics (17). Thus, the widely used contrast medium GdDTPA does not seem to

[1]Center for Pharmaceutical and Molecular Imaging, Department of Radiology, University of California, San Francisco, California.
[2]Department of Radiology, University of Vienna, Austria.
[3]Department of Radiology, Erasmus MC, University Medical Center Rotterdam, The Netherlands.
[4]Schering AG, Berlin, Germany.
[5]Department of Medical Imaging, University of Toronto, Canada.
Contract grant sponsor: Whitaker Foundation; Contract grant sponsor: Erwin Schrödinger Auslandsstipendium, Austria.
*Address reprint requests to: T.P.L.R., Department of Medical Imaging, University of Toronto, 150 College Street, Toronto, M5S 3EZ ON, Canada. E-mail: tim.roberts@utoronto.ca
Received June 5, 2003; Accepted January 30, 2004.
DOI 10.1002/jmri.20049
Published online in Wiley InterScience (www.interscience.wiley.com).

be promising for the purpose of quantitatively monitoring permeability changes in the microvasculature. On the other hand, because the more promising prototype MMCM, albumin-$(GdDTPA)_{30}$, is not suited for human use, several new MR contrast media are under vigorous development. Despite these research efforts, so far it is not known which size or molecular weight (MW) of a particular contrast medium would be best suited for tumor microvessel characterization. In particular, an ideal agent must show sensitivity to disease progression and responsiveness to interventional therapy, offering a wide dynamic range of target parameters such as permeability, and be amenable to clear-cut demonstrations of both positive and negative effects (change to noise ratio). Furthermore, for clinical applicability, such clear-cut resolution of permeability changes should ideally be derived from only a few minutes of dynamic imaging.

Therefore, the purpose of this study was to investigate different MR contrast media of various sizes/MWs in order to define the cutoff size that would be best suited to enable a reliable, quick, and precise tumor microvessel characterization, sensitive to changes associated with disease progression and therapeutic response. For this purpose, an established model of suppressing tumor angiogenesis was used: tumor neovascularization was blocked by means of an antivascular endothelial growth factor (VEGF) antibody in an experimental human breast cancer.

MATERIALS AND METHODS

Animal Model

The study was performed with the approval of the Institutional Committee for Animal Research and in accordance with the guidelines of the National Institutes of Health for the care and use of laboratory animals.

MD-MBA-435, a poorly differentiated human breast cancer cell line with high expression of VEGF, was implanted into 31 four-week-old female homozygous athymic rats (Harlan, Indianapolis, IN). Approximately 5×10^6 human breast cancer cells, MDA-MB-435 (Cell Culture Facility of the University of California, San Francisco), suspended in a total volume of 0.3 mL (1:1 mixed with Matrigel®; Collaborative Biomedical Products, Bedford, MA), were implanted in the mammary fat pad using a 25-Gauge needle (Abbott Laboratories, North Chicago, Ill). All animals were observed daily at the test facility for general appearance, behavior, and tumor growth. Baseline MRI was performed when tumors reached a size of 10–15 mm. Before MRI animals were anesthetized by intraperitoneal injection of 50 mg/kg sodium pentobarbital. A 25-Gauge butterfly catheter (Abbott Laboratories, North Chicago, IL) was inserted into the tail vein for contrast media injection. Rats were placed on a heated water pad to keep the body temperature at physiological levels. Immediately after the MRI examination 2 mL of saline was injected subcutaneously to avoid dehydration effects.

MRI

MRI was performed on animals using an Omega CSI-II superconducting system (Bruker Instruments, Fremont, CA) operating at 2 Tesla and equipped with Acustar S-150 self-shielded gradient coils. The rats were placed supine within a birdcage radio frequency coil (inner diameter = 4.5 cm, length = 7.6 cm). A phantom filled with diluted 0.01 mmol/liter gadopentetate dimeglumine was positioned in the field of view (FOV) to correct for potential spectrometer variation in each experiment. A series of precontrast images were acquired using an axial T1-weighted three-dimensional spoiled gradient-recalled (3D-SPGR) sequence with varying repetition times between 30 and 1000 msec; other parameters were TE = 1.4 msec, one excitation, matrix = $128 \times 128 \times 16$, FOV = $50 \times 50 \times 48$ mm, slice thickness = 3 mm, and flip angle (α) = 90°. These sequences were used to calculate baseline relaxation rates ($R_1 = 1/T1$) for blood and tumor by curve fitting. Dynamic contrast-enhanced MRI was performed using a T1-weighted 3D-SPGR sequence with a keyhole technique consisting of three initial precontrast and dynamic postcontrast images. When small- and medium-size MR contrast media (GdDTPA, ZK159560, ZK181220, Gadomer-17) were used, 37 postcontrast images were acquired with high temporal resolution using a keyhole technique with the following parameters: TR = 50 msec, TE = 1.4 msec, one signal acquired, matrix = $128 \times 64 \times 8$, FOV = $50 \times 50 \times 48$ mm, slice thickness = 3 mm, and acquisition time = 6 seconds per image. When MMCM (albumin-$(GdDTPA)_{30}$ or SHU555C) were used precontrast images were immediately followed by 30 dynamic 3D-SPGR postcontrast images with a high spatial resolution (matrix = $128 \times 128 \times 16$, otherwise identical parameters, acquisition time = 1 minute 42 seconds/sequence).

Table 1
Contrast Agents Administered (With Molecular Weights and Doses)

Contrast agent	MW	Dose
GdDTPA (Magnevist)	547Da	0.1 mmol/kg
ZK159560	8.7kDa	0.1 mmol/kg
Gadomer-17	17kDa	0.1 mmol/kg
ZK181220	25.9kDa	0.1 mmol/kg
Albumin-$(GdDTPA)_{30}$	92kDa	0.03 mmol/kg
USPIO (SHU555C)	–	2.5 mgFe/kg

MR Contrast Media

Six different media of different sizes and/or MW have been used in this study (Table 1).

GdDTPA has an MW of 547 and was injected on day 1 at a dose of 0.1 mmol/kg. GdDTPA has a distribution volume approximating the extracellular volume, its plasma disappearance is rapid and multiexponential, and its elimination occurred exclusively via the kidneys (18).

ZK159560 and ZK181220 are prototype MR contrast media developed by Schering AG (Berlin, Germany) and differ only by their MWs (ZK159560, 8.7 kDa; ZK181220, 25.9 kDa). Both ZK159560 and ZK181220 were injected at a dose of 0.1 mmol/kg.

Gadomer-17 is a prototype MR contrast medium from Schering AG (Berlin, Germany) with an MW of 17 kDa (19). Gadomer-17 has 24 Gd complexes bound to each

molecule; the distribution volume is 0.11 liter/kg. It is eliminated by the kidneys with only 4% remaining at 24 hours (19). The toxicity is low with an LD_{50} (lethal dose in 50% of the population) of more than 30 mmol/kg in the rat. Gadomer-17 was injected at a dose of 0.1 mmol/kg.

Albumin-$(GdDTPA)_{30}$ is a 92-kDa prototype of a water-soluble MMCM with 6 nm diameter, synthesized in our laboratory following the method of Ogan et al (20). Albumin-$(GdDTPA)_{30}$ has a distribution volume of 0.05 liter/kg (which closely approximates the blood volume) and a plasma half-life of three hours in rats, which produces nearly constant enhancement of normal tissues for 30 minutes or longer after injection. Albumin-$(GdDTPA)_{30}$ was injected on imaging day 1 at a dose of 0.03 mmol Gd/kg.

SHU555C (Schering AG, Berlin, Germany) consists of ultrasmall superparamagnetic iron oxide (USPIO) particles with a mean core size of 3–4 nm diameter and a total hydrodynamic diameter of ≈30 nm. The distribution volume of SHU555C is 0.04 liter/kg and the acute tolerance (in mice, i.v.) is >10 mmol/kg. The R1 (= 1/T1) of the agent in plasma is 22 $second^{-1}mM^{-1}$ Fe and the R2 (= 1/T2) is 65 $second^{-1}mM^{-1}Fe$ (at 20 MHz, 37°C). The mean plasma half-life in rats is about one hour, and the particles are taken up by the mononuclear phagocyte system. SHU555C was injected 24 hours after the albumin-$(GdDTPA)_{30}$ injection at a dose of 2.5 mg Fe/kg.

Experimental Protocol

After the baseline MR examinations, animals were randomly assigned to the drug treatment or control group. Each rat was then imaged with one of the two smaller agents, one of the two intermediate agents, and one of the two larger agents (day 0, intermediate; day 1, small, followed after at least two hours by large). Because of the lack of availability of ZK159560 and SHU555C compared to GdDTPA and albumin-GdDTPA, and the prototypical nature of the latter two, more animals were imaged with these better-characterized agents than their analogs of similar size category. Physiological saline (0.2 mL) was injected i.p. in rats belonging to the control group; the drug group was treated with an i.p. injection of 0.2 mL of monoclonal antibody (Mab)-VEGF antibody (Genentech, South San Francisco, CA). The i.p. injections were done on days 1, 4, and 7. The day following the seventh day of drug/saline treatment all animals were imaged a second time using the identical protocol applied for pretreatment assessment. All animals were killed after the second post-treatment MR examination by an intravenous overdose of 0.3 mL of pentobarbital.

MRI Data and Kinetic Analysis

Images were transferred to, processed, qualitatively examined, and quantitatively analyzed on a Sun Sparc Ultra-10 workstation (Sun Microsystems, Mountain View, CA) using the MR-Vision Software package (The MR-Vision Co., Menlo Park, CA). In each rat and at each time point, regions of interest (ROIs) were defined by a semiautomated threshold-based method in which the strongly contrast-enhancing pixels on a late postcontrast image were selected to represent the tumor periphery. ROIs were also drawn in the phantom and in the inferior vena cava (IVC). The dynamic signal responses were corrected for potential temporal spectrometer variation by dividing by the signal intensity (SI) of the phantom. Postcontrast R1 values were calculated based on the SI and knowledge of precontrast R1 values for each ROI. Differences between the precontrast and postcontrast R1 values at any time (ΔR1) were assumed to be proportional to the concentration of the contrast medium, either in the blood or in the tissue of interest (21–23). This method of ΔR1 determination is limited by the inherent assumption that the fully relaxed SI did not vary significantly on pre- and postcontrast SPGR images (23). The ΔR1 data from blood and tumor were used for kinetic analysis to estimate the coefficient of K^{PS} (mL $minute^{-1}$ 100 cc^{-1} of tissue) and the fPV (mL cc^{-1} of tissue). In brief, while the initial enhancement of relaxation in a voxel of tissue relates to the fractional blood volume, progressive tissue relaxation enhancement relates to contrast agent leak from the intravascular to the extravascular compartment. Constructing the ratio of tissue relaxation enhancement to reference vascular relaxation enhancement (from the IVC) allows approximate graphical visualization of fPV and permeability from the intercept and slope of the plot against time, respectively. Accurate estimations incorporating consideration of plasma tracer disappearance and bidirectional tracer transport between intra- and extravascular compartments are obtained from two-compartment bidirectional kinetic modeling.

All data fitting was performed using a nonlinear least squares numerical approach, implemented in Kaleidagraph 3.5 (Synergy Software, Reading, PA). Fit parameters fPV and K^{PS} are converted to units of mL/cc tissue (equivalent to the fraction given by the intercept of the plot of the ratio of tissue to vascular relaxation enhancement) and mL/100 g/minute (manageable units of volume transport per mass of tissue, derived by scaling fit units of tissue to vascular relaxation enhancement ratio, or fraction, per second, assuming a tissue density of 1 g/cc and rescaling from seconds to minutes).

Tumor volumes were calculated by approximate numerical integration: summation of the measured tumor area on each slice, multiplied by the slice thickness (3 mm).

Statistics

The paired two-tailed Student's *t*-test was used to compare mean K^{PS} and fPV values in the same tumors pre- and postintervention (drug or control) for each contrast medium. The two-tailed paired Student's *t*-test was used to calculate differences in the tumor volume over time in each rat. $P < 0.05$ was considered statistically significant.

RESULTS

Implanted tumors grew to a size of approximately 1.5 cm within 14 days. The final study population con-

Table 2
Study Sample Sizes for Each Contrast Agent and Treatment Arm

	Control	Drug group
GdDTPA	9	13
ZK159560	0	7
Gadomer-17	5	7
ZK181220	5	6
SHU555C	6	6
Albumin-$(GdDTPA)_{30}$	12	19

sisted of 31 rats, which were randomly assigned to control or drug-treated groups (Table 2).

Taking all animals together, tumor volumes at baseline examination were not significantly different ($P = 0.49$) between the drug-treated (1076 ± 763 mm^3) and control (777 ± 240 mm^3) groups. Tumors continued growing in both animal groups, from 777 ± 240 to 2594 ± 1121 in the control group, and from 1076 ± 763 to 1830 ± 1408 in the drug-treated group. Hence, tumors grew significantly faster ($P < 0.0005$) in the control group (calculated tumor growth ratio = 3.3 ± 1.0) than in the drug-treated group (tumor growth ratio = 1.79 ± 0.7).

Mean K^{PS} and fPV values at baseline and at the follow-up examination using all contrast media are listed in Table 3 for both groups, drug-treated and control animals. In the Mab-VEGF antibody-treated group, mean K^{PS} and fPV values decreased significantly ($P < 0.05$) from baseline values using any of the four intermediate or larger-size agent: albumin-$(GdDTPA)_{30}$, SHU555C, Gadomer-17, or ZK181220. Using smaller agents, ZK159560 and GdDTPA, mean K^{PS} and fPV values between pre- and post-treatment exam did not reach statistical significance ($P > 0.05$). In the control groups, mean K^{PS} and fPV values did not reach statistical significance for any of the contrast media used.

DISCUSSION

This study shows that suppression of tumor neoangiogenesis leads to a considerable slowdown in tumor growth within one week of treatment. Although the implanted human breast cancers continued to grow in both groups, no matter if the animals were treated with saline (control group) or a Mab-VEGF antibody (drug group), the tumor growth ratio was statistically significantly ($P < 0.0005$) smaller in the drug-treated group than in the control group.

VEGF is considered to be one of the most important promoters of tumor neoangiogenesis (24–27). VEGF and its receptors are upregulated in early phases of tumor neovascularization, thereby stimulating endothelial cell proliferation and migration. Also, VEGF has crucial effects on the endothelial wall integrity, gaps and channels within endothelial cells are numerically increased, and tight junctions between the cells are loosened. Indeed, VEGF, also known as vascular permeability factor (VPF), induces vessel hyperpermeability, which leads to an extravasation of plasma proteins and the formation of a matrix that is favorable for blood vessel growth (28,29). Thus, inhibition of VEGF is accompanied by a decrease in microvascular permeability to proteins and macromolecules and a suppression of neoangiogenesis, both facts nicely demonstrated in the present study.

It is clear, however, that the property of microvascular permeability must depend upon the physical characteristics (size) of the tracer solutes. Whereas SMCM diffuse through normal and injured vessel walls, MMCM remain strongly intravascular within normal vessels. But as soon as the vessel wall integrity is disrupted—no matter if the underlying cause is neoplastic, inflammatory, or toxic—MMCM diffuse into the interstitial space (30–32). Albumin-$(GdDTPA)_{30}$ has been used successfully as a prototype MMCM (≈92 kDa) to define microvascular characteristics in several experimental studies (15,33). These include different physiological and pathological conditions such as tumors (16,33–35), inflammation (31), myocardial ischemic states (32), wound healing (36), and toxin exposure. The incomplete elimination of the gadolinium part of this compound from the body and its potential immu-

Table 3
Mean Permeability Values (K^{PS}) and Fractional Plasma Volume (fPV) Using Different Contrast Media for the Control (Saline) and Drug-Treated (Mab-VEGF Antibody) Groups

	Control		Drug	
	Pre	Post	Pre	Post
K^{PS}				
GdDTPA	6.75 ± 7.05	7.35 ± 8.99	3.27 ± 18.9	2.56 ± 3.16
ZK159560	Not studied	Not studied	1.34 ± 1.47	2.81 ± 1.65
Gadomer-17	1.121 ± 0.358	1.205 ± 0.307	1.064 ± 0.420	0.445 ± 0.234*
ZK181220	0.418 ± 0.307	0.430 ± 0.199	0.469 ± 0.348	0.196 ± 0.160*
SHU555C	0.010 ± 0.009	0.021 ± 0.025	0.018 ± 0.016	0.002 ± 0.003*
Albumin-$(GdDTPA)_{30}$	0.016 ± 0.011	0.012 ± 0.020	0.019 ± 0.020	0.007 ± 0.010*
fPV				
GdDTPA	34.4 ± 18.4	42.2 ± 17.0	38.8 ± 13.2	33.8 ± 14.1
ZK159560	Not studied	Not studied	9.1 ± 10.0	9.5 ± 4.4
Gadomer-17	11.4 ± 6.1	14.7 ± 4.0	12.3 ± 6.3	6.1 ± 4.4*
ZK181220	13.5 ± 5.8	10.5 ± 4.7	10.4 ± 3.2	6.3 ± 3.3*
SHU555C	4.4 ± 1.4	5.1 ± 3.0	5.4 ± 2.1	3.0 ± 1.0*
Albumin-$(GdDTPA)_{30}$	6.1 ± 2.8	6.1 ± 1.5	7.25 ± 2.43	4.33 ± 1.46*

* = Statistically significant from baseline ($P < .05$).
K^{PS} = coefficient of permeability surface area product (ml/min/100cc tissue); fPV = fractional plasma volume (%); Drug = Mab-VEGF antibody.

nologic response, however, hinder its clinical use (20). Recently, USPIO particles have been shown in an animal model to have the potential for defining tumor microvessel characteristics (16). K^{PS} and fPV generated with USPIO correlated strongly and statistically significantly ($P < 0.01$) with albumin-$(GdDTPA)_{30}$-derived K^{PS} and fPV values using dynamic MRI and a bidirectional kinetic model (16). However, both albumin-$(GdDTPA)_{30}$ and USPIO suffer from very low absolute signal enhancement due to very low rates of contrast media extravasation. Consequently, long scan observation periods are necessitated to observe significant enhancement above the image noise level.

Using SMCM, like GdDTPA (MW = 547) and ZK159560 (MW = 8.7 kDa), for determining K^{PS} and fPV, no statistically significant correlation between pre- and post-Mab-VEGF antibody-treated subjects was found, largely due to the very rapid and very pronounced signal enhancement observed, which precluded simple kinetic modeling, yielding estimates of fPV and K^{PS} with high uncertainties and large within group standard deviations. In some sense, kinetic modeling of dynamic enhancement with such agents can be considered to be limited by ceiling effects, in contrast to the floor limits associated with albumin-GdDTPA and USPIO.

Hence, the development of intermediate-size agents might facilitate considerably the monitoring and calculation of effects of changes in K^{PS} following antiangiogenic therapy. Indeed, using Gadomer-17, in comparison to GdDTPA and albumin-GdDTPA, Su et al (37) have demonstrated MR determination of microvascular permeability in an N-ethyl-N-nitrosourea (ENU) model of breast cancer in the rat. In their study, they show that the intermediate permeability of Gadomer-17 was able to distinguish low-grade from high-grade cancers, but unable to resolve benign from low-grade, because of permeability range overlap. GdDTPA failed to differentiate between low- and high-grade malignant tumors. Albumin could differentiate both, high- from low-grade malignant tumors and benign from malignant tumors, but its low contrast-to-noise ratio raised major concerns.

This study in fact shows that intermediate-size contrast media with an MW in the range of 20–30 kDa also allow tumor microvessel characterization, in a therapy model, in a fashion similar to that in larger macromolecules. Both medium-size contrast media, Gadomer-17 (MW = 17 kDa) and ZK181 (MW = 25.9 kDa), revealed a statistically significant difference ($P < 0.05$) in permeability and fPV values between pre- and post-treatment examinations.

Additionally, resolution of such treatment effects was in fact facilitated using Gadomer-17 and ZK181220 by the greater degree of enhancement, or rate of contrast media extravasation, compared to the prototype MMCM. In such a way, imaging precision did not appear to limit permeability estimation to the same extent as seen with the low leak rates and very small signal enhancement of MMCM, comparable to image noise levels. Consequently, for MMCM contrast media leakage over a period of up to one hour is generally required for unambiguous observation of progressive signal enhancement (as opposed to mere image noise). Intermediate agents demonstrated substantial (≈100%) signal enhancement within five minutes. This observation

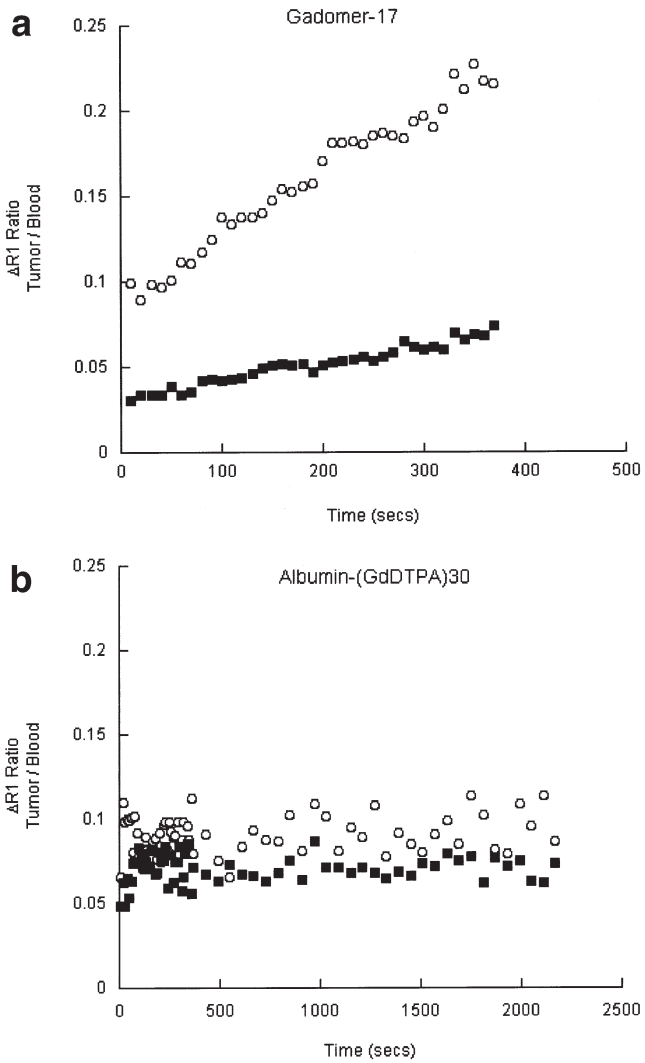

Figure 1. **a:** ΔR1 ratios in tumors pre- (○) and post- (■) Mab-VEGF antibody treatment over one week demonstrate substantial signal enhancement within five minutes using an intermediate agent, represented here by Gadomer-17. **b:** In contrast, using MMCM (i.e., albumin-$(GdDTPA)_{30}$) imaging precision is limited because of very small signal enhancement, comparable to image noise levels.

alone is of considerable practical utility when translating to a clinical setting (Fig. 1).

Clarity of resolution of treatment effects with Gadomer-17 and ZK181220 can be further documented by considering individual instead of group effects. In all seven rats treated with Mab-VEGF antibody, Gadomer-17-K^{PS} estimates decrease over the treatment period (Fig. 2). While group comparison showed a significant decrease in mean K^{PS} for albumin-$(GdDTPA)_{30}$, there was not a similar 100% concordance observed in the individual data, in which only 76% of cases showed a decrease in K^{PS}. In general, as can be seen from Fig. 3, there is an approximately exponential decrease in K^{PS} values with increasing MW. In fact, the correlation coefficient of ln(K) vs. MW is r = −0.98, indicating a strong negative correlation when considering the pooled pretreatment values from both control and treated groups. This can be rationalized intuitively if one considers the

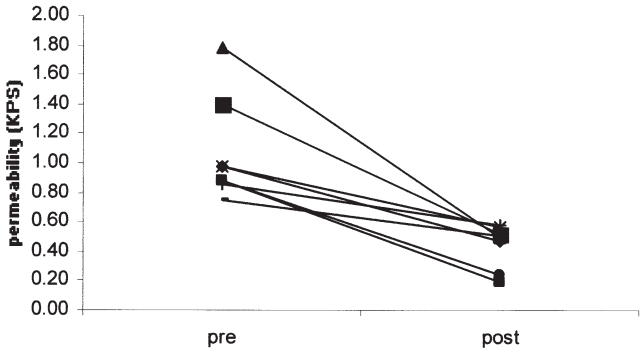

Figure 2. Individual permeability values, K^{PS} (μL minute^{-1} 100 cc^{-1} of tissue) before and after one week of drug treatment in the group imaged with Gadomer-17.

impediments to larger molecule transport, including slower diffusion (to the extent that diffusion is a mechanism), greater sensitivity to elevated tumor interstitial pressure (to the extent that convection is the transport mechanism), and reduced access to fenestrae in the vascular wall.

The intermediate agents were not, however, so leaky (compared to GdDTPA, for example) that documentation of progressive enhancement was rendered impractical because of high first-pass extraction fraction (≈50% for GdDTPA). However, both intermediate contrast media did overestimate fPV (as did the SMCM) when compared to the bigger reference MMCM, albumin-$(GdDTPA)_{30}$ and SHU555C. It is possible that this overestimation can in part be attributed to partial first-pass extravasation.

There are three possible explanations for the apparent lack of utility of permeability assessment using SMCM to document treatment success in this study: 1) insufficient image acquisition rates to capture the more rapid dynamics; 2) inappropriate modeling, violating extraction fraction assumptions; and 3) biological irrelevance, i.e., K^{PS} to SMCM may not in fact be affected by Mab-VEGF antibody action. Although there have been a number of reports of the successful use of dynamic contrast-enhanced MRI for characterizing tumor microvasculature phenomena in clinical patients, most of these methodologies do not rely on the elucidation of a parameter with physiologically specific interpretation (such as microvascular permeability). Rather, they rely on observed or derived descriptors of signal change, typically sensitive to a combination of perfusion, vascular volume, and microvascular permeability. Examples include the use of first-pass T2*-based imaging (measuring the peak change in 1/T2* observed) (38) or constructions such as the initial area under the curve (IAUC) (39). Both can be demonstrated to be robustly determined and of some clinical utility, but lack the above physiologically specific interpretation and, as such, are subject to a number of potential confounds (e.g., systemic changes in cardiac output or blood pressure as well as local perfusion alterations that may be incidental to the mechanism of action of the drug).

In conclusion, the quantitative use of microvascular permeability estimation as an index of antiangiogenic therapeutic efficacy is constrained by two limits. If the MW of the tracer is too small, estimates of fPV and K^{PS} have high uncertainties and true values are usually overestimated considerably. If, on the other hand, the MW is too big, contrast media enhancement of tumors is confounded by image noise and difficult or even impossible to determine.

A successful compromise appears delivered by intermediate-size agents, such as Gadomer-17, whereby a substantial dynamic range of permeability offers clear delineation of treatment effects, much less limited by imaging precision, and thus practically requiring shorter observation times to observe significant enhancement.

In summary, therapeutic effects of a Mab-VEGF antibody on tumor microvessel characteristics can be monitored by dynamic MRI. Intermediate-size agents, such as Gadomer-17, offer a substantial dynamic range and are less limited by imaging precision and therefore should be considered a practical alternative

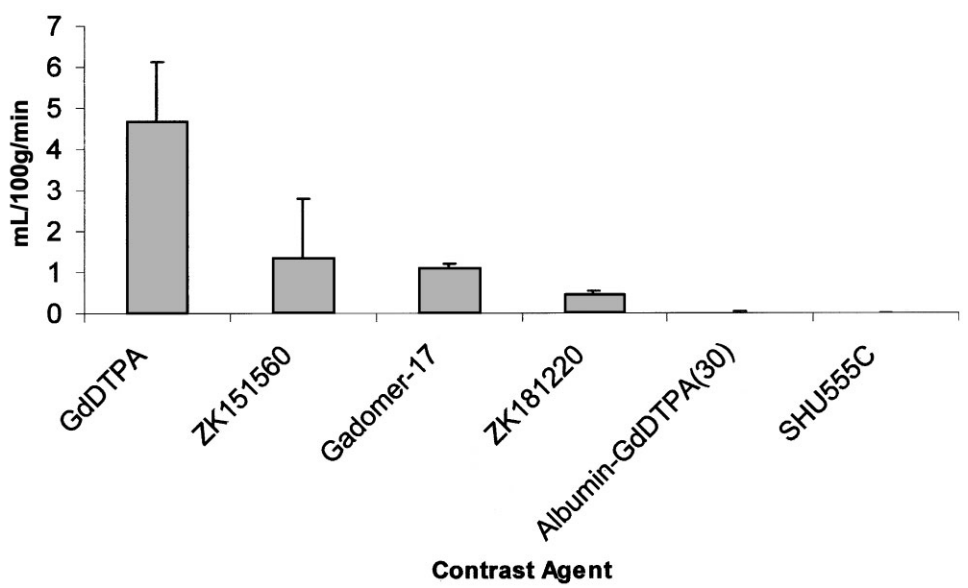

Figure 3. Pooled pretreatment (precontrol) K^{PS} values as a function of MW indicate an approximately exponential decrease in K^{PS} with MW. The correlation coefficient between ln(K) and MW is r = −0.98.

to monitor antiangiogenesis treatment effects in a clinical setting.

ACKNOWLEDGMENTS

We thank Schering AG for the generous donation of contrast media, and Genentech Inc. (South San Francisco, CA) for the Mab-VEGF antibody. This research was supported by a grant from the Whitaker Foundation (to T.P.L.R.). K.T. was supported by the Erwin Schrödinger Auslandsstipendium, Austria.

REFERENCES

1. Fontanini G, Lucchi M, Vignati S, et al. Angiogenesis as a prognostic indicator of survival in non-small-cell lung carcinoma: a prospective study. J Natl Cancer Inst 1997;89:881–886.
2. Takahashi Y, Kitadai Y, Bucana CD, Cleary KR, Ellis LM. Expression of vascular endothelial growth factor and its receptor, KDR, correlates with vascularity, metastasis, and proliferation of human colon cancer. Cancer Res 1995;55:3964–3968.
3. Brock CS, Lee SM. Anti-angiogenic strategies and vascular targeting in the treatment of lung cancer. Eur Respir J 2002;19:557–570.
4. Cherrington JM, Strawn LM, Shawver LK. New paradigms for the treatment of cancer: the role of anti-angiogenesis agents. Adv Cancer Res 2000;79:1–38.
5. Folkman J. Angiogenesis and breast cancer [Editorial; Comment]. J Clin Oncol 1994;12:441–443.
6. Hoekman K. SU6668, a multitargeted angiogenesis inhibitor. Cancer J 2001;7(Suppl 3):S134–S138.
7. Strawn LM, McMahon G, App H, et al. Flk-1 as a target for tumor growth inhibition. Cancer Res 1996;56:3540–3545.
8. Varner JA, Cheresh DA. Integrins and cancer. Curr Opin Cell Biol 1996;8:724–730.
9. Gutheil JC, Campbell TN, Pierce PR, et al. Targeted antiangiogenic therapy for cancer using Vitaxin: a humanized monoclonal antibody to the integrin alphavbeta3. Clin Cancer Res 2000;6:3056–3061.
10. Fujita M, Hayashi I, Yamashina S, Itoman M, Majima M. Blockade of angiotensin AT1a receptor signaling reduces tumor growth, angiogenesis, and metastasis. Biochem Biophys Res Commun 2002; 294:441–447.
11. Brooks PC, Montgomery AMP, Rosenfeld M, et al. Integrin alpha-(v)beta(3) antagonists promote tumor-regression by inducing apoptosis of angiogenic blood vessels. Cell 1994;92:391–400.
12. Bruns CJ, Solorzano CC, Harbison MT, et al. Blockade of the epidermal growth factor receptor signaling by a novel tyrosine kinase inhibitor leads to apoptosis of endothelial cells and therapy of human pancreatic carcinoma. Cancer Res 2000;60:2926–2935.
13. Roberts WG, Palade GE. Neovasculature induced by vascular endothelial growth factor is fenestrated. Cancer Res 1997;57:765–772.
14. Qu H, Nagy JA, Senger DR, Dvorak HF, Dvorak AM. Ultrastructural localization of vascular permeability factor/vascular endothelial growth factor (VPF/VEGF) to the albuminal plasma membrane and vesiculovacuolar organelles of tumor microvascular endothelium. J Histochem Cytochem 1995;43:381–389.
15. Shames DM, Kuwatsuru R, Vexler V, Muhler A, Brasch RC. Measurement of capillary permeability to macromolecules by dynamic magnetic resonance imaging—a quantitative noninvasive technique. Magn Reson Med 1993;29:616–622.
16. Turetschek K, Huber S, Floyd E, et al. MRI characterization of microvessels in experimental breast tumors using a particulate contrast agent with histopathologic correlation. Radiology 2001; 218:562–569.
17. Turetschek K, Preda A, Floyd E, et al. MRI monitoring of tumor response following angiogenesis inhibition in an experimental human breast cancer model. Eur J Nucl Med Mol Imaging 2003;30: 448–455.
18. Weinmann H, Laniado M, Mützel W. Pharmacocinetics of Gd-DTPA/dimeglumine after intravenous injection into healthy volunteers. Physiol Chem Phys Med NMR 1984;16:167–172.
19. Adam G, Neuerburg J, Spuentrup E, Muehler A, Schere K, Guenther R. Dynamic contrast enhanced MR-imaging properties of gadobutol, gadolinium-DTPA-polylysine, and Gd-DTPA-cascade-polymer. Magn Reson Med 1994;32:622–628.
20. Ogan M, Schmiedl U, Moseley M, Grodd W, Paajenen H, Brasch RC. Albumin labeled with Gd-DTPA: an intravascular contrast enhancing agent for magnetic resonance blood pool imaging: preparation and characterization. Inv Radiol 1987;22:665–671.
21. Wedeking P, Sotak CH, Telser J, Kumar K, Chang CA, Tweedle MF. Quantitative dependence of MR signal intensity on tissue concentration of Gd(HP-DO3A) in the nephrectomized rat. Magn Reson Imaging 1992;10:97–108.
22. Schwickert HC, Roberts TP, Shames DM, et al. Quantification of liver blood volume: comparison of ultra short TI inversion recovery echo planar imaging (ULSTIR-EPI), with dynamic 3D-gradient recalled echo imaging. Magn Reson Med 1995;34:845–852.
23. Roberts TP. Physiologic measurements by contrast-enhanced MR imaging: expectations and limitations. J Magn Reson Imaging 1997;7:82–90.
24. Martiny-Baron G, Marmé D. VEGF-mediated tumour angiogenesis: a new target for cancer therapy. Curr Opin Biotechnol 1995;6:675–680.
25. Arii S, Mori A, Uchida S, Fujimoto K, Shimada Y, Imamura M. Implication of vascular endothelial growth factor in the development and metastasis of human cancers. Hum Cell 1999;12:25–30.
26. Drevs J, Hofmann I, Hugenschmidt H, et al. Effects of PTK787/ZK 222584, a specific inhibitor of vascular endothelial growth factor receptor tyrosine kinases, on primary tumor, metastasis, vessel density, and blood flow in a murine renal cell carcinoma model. Cancer Res 2000;60:4819–4824.
27. Karkkainen MJ, Petrova TV. Vascular endothelial growth factor receptors in the regulation of angiogenesis and lymphangiogenesis. Oncogene 2000;19:5598–5605.
28. Claffey KP, Robinson GS. Regulation of VEGF/VPF expression in tumor cells: consequences for tumor growth and metastasis. Cancer Metastasis Rev 1996;15:165–176.
29. Veikkola T, Karkkainen M, Claesson-Welsh L, Alitalo K. Regulation of angiogenesis via vascular endothelial growth factor receptors. Cancer Res 2000;60:203–212.
30. Brasch R, Pham C, Shames D, et al. Assessing tumor angiogenesis using macromolecular MR imaging contrast media. J Magn Reson Imaging 1997;7:68–74.
31. Berthezene Y, Vexler V, Kuwatsuru R, et al. Differentiation of alveolitis and pulmonary fibrosis with a macromolecular MR imaging contrast agent. Radiology 1992;185:97–103.
32. Saeed M, van Dijke CF, Mann JS, et al. Histologic confirmation of microvascular hyperpermeability to macromolecular MR contrast medium in reperfused myocardial infarction. J Magn Reson Imaging 1998;8:561–567.
33. Daldrup H, Shames DM, Wendland M, et al. Correlation of dynamic contrast-enhanced MR imaging with histologic tumor grade: comparison of macromolecular and small-molecular contrast media. AJR Am J Roentgenol 1998;171:941–949.
34. Schwickert HC, Stiskal M, Roberts TP, et al. Contrast-enhanced MR imaging assessment of tumor capillary permeability: effect of irradiation on delivery of chemotherapy. Radiology 1996;198:893–898.
35. Gossmann A, Okuhata Y, Shames DM, et al. Prostate cancer tumor grade differentiation with dynamic contrast-enhanced MR imaging in the rat: comparison of macromolecular and small-molecular contrast media—preliminary experience. Radiology 1999;213:265–272.
36. Helbich T, Roberts TPL, Rollins MD, et al. Non-invasive assessment of wound healing angiogenesis with contrast enhanced MRI. Acad Radiol 2002;9(Suppl 1):145–147.
37. Su M-Y, Wang Z, Carpernter PM, Lao X, Muhler A, Nalcioglu O. Characterization of N-ethyl-N-nitrosourea-induced malignant and benign breast tumors in rats by using three MR contrast agents. J Magn Reson Imaging 1999;9:177–186.
38. Kuhl C, Bieling H, Gieseke J, et al. Breast neoplasms: T2* susceptibility-contrast, first-pass perfusion MR imaging. Radiology 1997; 202:87–95.
39. Evelhoch J. Key factors in the acquisition of contrast kinetic data for oncology. J Magn Reson Imaging 1999;10:254–259.